Visualization and Quantitative Evaluation of Eddy Current Loss in Bar-Wound Type Permanent Magnet Synchronous Motor for Mild-Hybrid Vehicles

Masahiro Aoyama, *Member, IEEE*, and Jianing Deng

***Abstract*—This paper describes the conductor eddy current loss that occurs in a permanent magnet type synchronous motor with a distributed winding stator using a rectangular copper wire designed for mild hybrid system applications for small vehicles. Compared with the conventional round wire inserter method, the space factor can be improved and the coil-end length can be shortened by applying a so-called hairpin windings using a pre-formed into hairpin shape of bar conductor, and as a result, DC current resistance of the armature winding can be reduced. However, since the conductor cross-sectional area tends to increases, the conductor eddy current loss generated by the space harmonics linkage becomes too large to ignore. In order to study the reduction of the conductor eddy current loss, it is important to visualize the spatial leakage flux distribution which causes loss and finely analyze how the magnetic path is formed. Therefore, analysis of the conductor eddy current loss distribution generated in the bar-wound conductor is performed using the CAE model that faithfully reproduces the coil-end shape of the actual machine. Furthermore, it was qualitatively clarified what ratio of conductor eddy current loss at various driving points. Finally, the results of preliminary study on reduction of conductor eddy current loss are reported.**

***Index Terms*—Conductor eddy current loss, hairpin windings type permanent magnet synchronous motor, leakage magnetic flux.**

I. Introduction

TODAY, electrification is being promoted as a national policy in each country as a countermeasure for global environmental load reduction in the transportation equipment field. The key components for the electrification technology of automobiles are a motor as the traction, a battery for energy storage, an inverter for energy management, and control algorism to integrate them. Among these key technologies, the motor serving as the traction is very important component because it greatly affects the drive performance of the vehicle on which it is mounted. Today, an induction motors and a permanent magnet synchronous motors are widely used as motors for driving electric vehicles. A suitable motor is selected as either an induction machine or a synchronous machine depending on the driving performance of the electric vehicle and the application or the system of the hybrid vehicle. In the case of compact-size vehicles, in addition to securing the climbing performance and acceleration, space constraints at the time of on-vehicle installation and weight reduction of parts are very important. From the viewpoint of giving priority to torque density, in the case of a compact-size vehicle, a permanent magnet synchronous motor (PMSM) is usually employed. In order to realize the high torque density of PMSM, shortening of the coil-end is important in addition to the adoption of the permanent magnet (PM) having a high residual magnetic flux density. In order to further increase the output, it is necessary to drive the motor at the high speed. In the case of a compact-size vehicle, it is required to have both the high torque and the high output mentioned above. Among the former, a concentrated winding stator can be considered as a method for shortening the coil-end length. But in the case of this stator type, since a large number of space harmonics are superimposed in this winding structure, the iron loss increases at high rotation speed, and motor efficiency decreases. In addition, the concentrated winding stator type is not suitable for small vehicle applications because the reluctance torque is lower than that of the distributed winding stator type. As the technique for shortening the coil-end length in the distributed winding stator type, there is a bar-wound conductor type, so-called hairpin windings [1], [2]. In the case of the bar-wound conductor type, a flat rectangular copper wire preformed into a hairpin shape is contained in the slot, and then the open side is welded to form a coil. Therefore, the space factor can be improved and the coil-end length can be shortened as compared with the method of inserting, and as a result, DC copper loss can be reduced. In particular, the PMSM applied the bar-wound coil type provided with the above-mentioned features maximizes the merit of high

Manuscript was submitted for review on 12, July, 2019.

The points related to the electromagnetic field analysis in this research was supported by the Japan Automobile Manufactures Association, Inc., using Supercomputer "K" of RIKEN. (Grant Number hp170150)

Masahiro Aoyama was with SUZUKI Motor Corporation, Shizuoka, JAPAN. He is now with the Department of Engineering, Shizuoka University, 3-5-1 Johoku Naka-ku, Hamamatsu, Shizuoka, JAPAN (e-mail: aoyama.masahiro@shizuoka.ac.jp).

Deng Jianing was with SUZUKI Motor Corporation, Shizuoka, JAPAN. He is now with DENSO Corporation, Aichi, 1-1 Showa-cho, Kariya, Aichi, JAPAN (e-mail: Deng.Jianing1082@gmail.com).

Digital Object Identifier 10.30941/CESTEMS.2019.00035

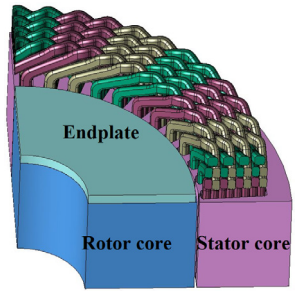

(a) CAE model.

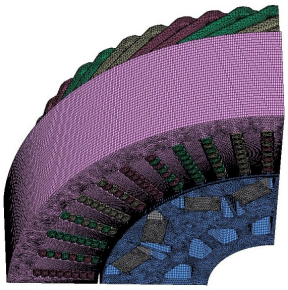

(b) Mesh model without air-region.

(c) Actual prototype.

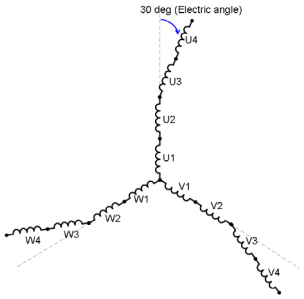

(d) Zig-zag winding connection.

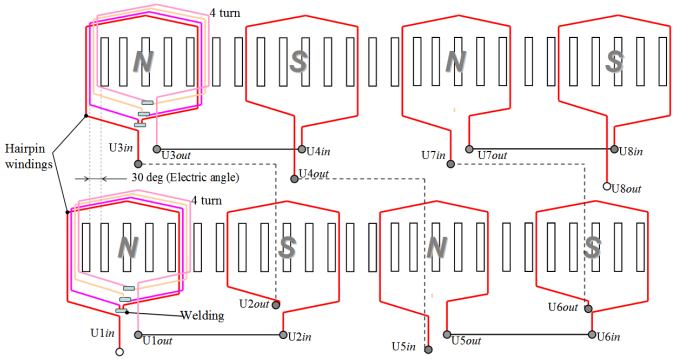

(e) U-phase coil connection diagram for 4-poles.

Fig. 1. CAE model and actual prototype.

torque density and small volume when mounted in a limited space such as an electric vehicles [3], [4]. This is great advantages compared to the conventional round-wire inserter method. Other hand, the use of a rectangular copper wire tends to increase the conductor cross-sectional area. The high torque density motor is designed to be driven in the magnetic saturation region of the magnetic steel sheet at a certain load or more, so the spatial leakage flux is easily to occur. This fact means that interlinking flux of spatial leakage flux is generated in the rectangular copper wire to cause conductor eddy current loss. When, the motor is designed to rotate at a high speed for higher output, the influence of its loss appears even more remarkably [5]. Since it is difficult to directly measure eddy current loss in hairpin coil, it is necessary to analyze finely in electromagnetic field analysis. However, as far as the authors know, a large-scale electromagnetic field analysis with high spec workstation is required, so the method is limited to estimation of eddy current loss in the coil modeled simply [6], [7]. On the other hand, with regard to iron loss, as described in Ref. [8], [9], research on improvement of iron loss calculation accuracy has been actively conducted by new calculation

TABLE I
MAIN SPECIFICATIONS OF PROTOTYPE.

Number of rotor poles	8
Number of stator slots	48
Outer diameter of stator core	125 mm
Radial-air-gap length	0.6 mm
Stack length of core	51.8 mm
Maximum rotational speed	15,000 r/min
Maximum torque, output	30 Nm, 10 kW
Maximum armature current	150 A_{rms}(Maximum), 75 A_{rms} (Rated)
Cooling method	Water cooling in housing
Number of armature coil-turn	8 turn / slot
Armature winding connection	4 series - 2 parallel
Conductor cross section	4.2 mm^2 / coil
Electric magnetic steel seat	35A230
Permanent magnet	N48TS-GR (Shinetsu chemical)

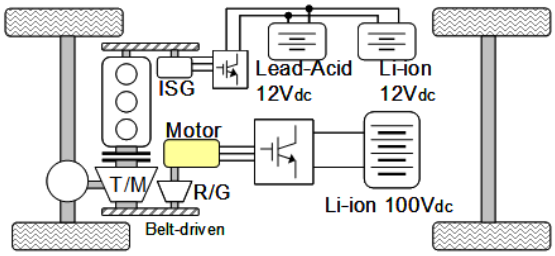

Fig. 2. P3 type hybrid system applied proposed motor.

methods such as a play model modeling the magnetic characteristics of materials in recent years.

In view of these problems, large-scale electromagnetic field analysis is performed using the CAE model that accurately models the coil shape of the real machine. At some typical drive point of the electric motor, spatial leakage flux is visualized. In addition, the conductor eddy current loss is quantitatively grasped. Furthermore, in order to grasp which part of the bar-wound conductor, e.g., coil-end part or embedded slot part, has the large amount of conductor eddy current loss, the conductor eddy current loss was determined quantitatively at each of the two parts of the conductor part enclosed within the slots and that of the coil-end part. Based on these results, preliminary research of eddy current loss reduction was conducted with divided bar-wound coil technique.

II. FE-ANALYSIS MODELING

A. Machine Design

Fig. 1 (a) shows the CAE model for electromagnetic field analysis and Fig. 1 (b) shows the mesh model without air-region. As can be seen by comparing this CAE model with the actual machine in Fig. 1 (c), it can be seen that the coil-end portion of the armature winding is strictly modeled. As a result, as can be inferred from the mesh model of Fig. 1 (b), the mesh model becomes enormous, and numerically, the number of nodes and that of elements in the meshed CAE model are 1,452,615 and 2,962,666, respectively. Here, the armature winding of the bar conductor is connected by so-called zig-zag

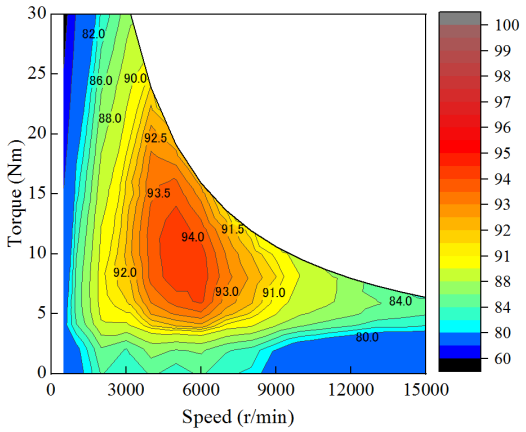

(a) Efficiency map in motoring under DC bus 100 V_{dc}.

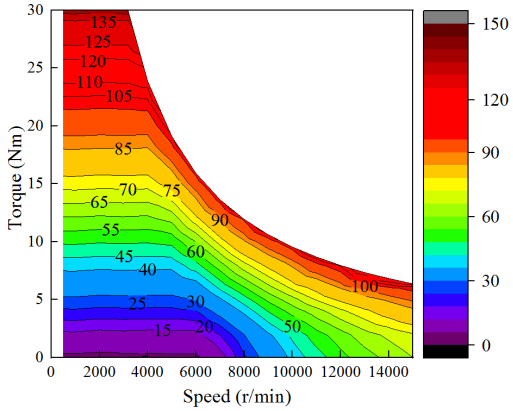

(b) Current norm map in motoring under DC bus 100 V_{dc}.

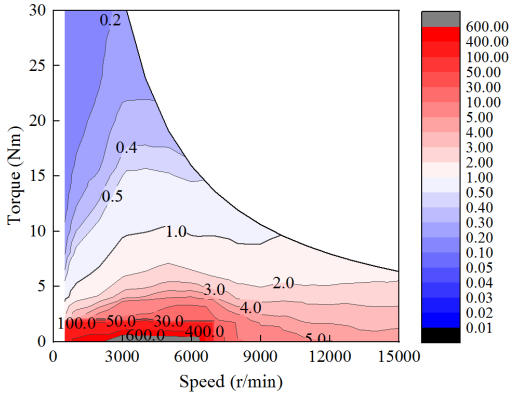

(c) Loss ratio map of iron loss and copper loss under DC bus 100 V_{dc}.

Fig. 3. Experimental test results using actual prototype.

winding as shown in Fig. 1 (d). The more detailed connection diagram for U-phase zig-zag winding is shown in Fig. 1 (e). It is composed of the total of 8 turns per pole by winding 4 turns with short-pitch winding, then shifting it by 1 slot and winding in the same way. Similarly, in the case of the V-phase and the W-phase, they are arranged with an electrical phase difference of 120 degrees. Therefore, there is a slot in which coils of different phase are included in one slot. The effect equivalent to skew can be obtained by connecting in series with the coil that is shifted by an electrical angle of 30 deg. In this case, it is equivalent to shift of one tooth with the mechanical angle of 7.5 deg. Table I shows the main specifications of prototype. This is the motor developed for low voltage hybrid system (generally called P3 type) application as shown in Fig. 2. As a feature of this hybrid system, the improvement of power performance and the improvement of fuel efficiency are obtained by using this motor to compensate for the torque loss at the time of shift of AMT (Automated Manual Transmission). By attaching the structure to the final stage of the AMT via a reduction gear, miniaturization is achieved with the low torque, high speed rotation type motor. This motor is an interior-permanent-magnet-synchronous-motor (IPMSM) with 8 poles and 48 slots which number of slots per pole per phase q = 2. Another main specifications of this motor are listed in Table I. The bar conductor is a flat wire having an AIW insulating film and has a rectangular cross section of 1.6 mm * 2.7 mm in size. The space factor of coil is 78.7 %, which is higher than that of the round wire inserter method. Since the armature winding has the short-pitch winding as shown in Fig. 1 (e), the torque is lower than that of the full-pitch winding due to the decrease in the number of armature interlinkage magnetic fluxes. However, the torque ripple can be greatly reduced by the zig-zag winding structure equivalent to the skew.

B. Drive Characteristics of Actual Prototype

Fig. 3 shows the experimental test results of the adjustable speed characteristics, the efficiency map in motoring, the armature current norm map, and the iron loss per copper loss ratio map using the actual machine of Fig. 1 (c). The test conditions are the DC bus voltage of 100 V_{dc} and the voltage utilization rate of 96 % upper limit, sinusoidal wave PWM modulation below the base rotation speed, and overmodulation and rectangular control above the base rotation speed. Below the base rotation speed, the reluctance torque is actively used under MTPA (Maximum Torque Per Ampere) control, and when the driving point is higher than the base rotation speed, the dq-axis current vector is driven by the norm that gives the maximum torque keeping within the voltage limited ellipse. Here, the high efficiency area at the high speed range side is narrow compared with a general IPMSM, because it is easy to magnetically saturate in order to put top priority on miniaturization and weight reduction, but it is also designed with high torque density and output power density. Fig. 3 (c) represents the ratio of the copper loss (W_c) to the iron loss (W_i). When W_i equal W_c, the value of copper loss and that of iron loss are equal. Also, W_i per W_c > 1.0 means a driving area with a high iron loss ratio, and vice versa means large copper loss area compared with the iron loss. At the low rotation speed with high load condition, the copper loss is dominant (W_i per W_c <1.0) because the norm of armature current is large to get high torque with armature magnetic flux, so the efficiency decreases. It is understood that the space factor improvement of armature coil and shortening the circumferential length of the coil-end is important to reduce the copper loss. Especially, in this motor model, the efficiency at the high rotation speed with low load condition is remarkably lowered. Because it is the low-voltage hybrid system such as 100-V_{dc}, the armature current phase is greatly advanced in the high rotation speed range, and magnetic field is strongly weaken with negative d-axis current norm. For the above reasons, the magnetic flux in the air-gap is greatly distorted and the iron loss is extremely increased. Here, in the

Table II
FE-ANALYSIS CONDITIONS AT TYPICAL OPERATING POINT.

Speed (r/min)	Armature current (A_{rms})	Current phase (deg)
3,183	137.3	44.0
9,000	56.0	73.0
15,000	127.0	81.5

Table III
COMPARISON WITH MEASURED AND ANALYSIS RESULTS WITH CONDUCTOR EDDY CURRENT LOSS CONSIDERATION.

Speed (r/min)	Measured (Nm)	FEA (Nm)
3,183	30.0	31.6
9,000	5.0	5.6
15,000	6.9	8.8

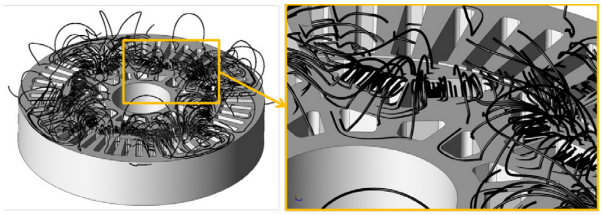

(a) 3,183 r/min. (137.3 A_{rms} and β = 44.0 deg)

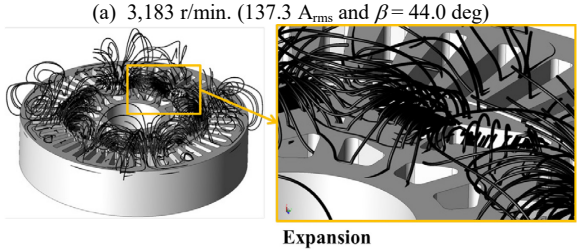

(b) 9,000 r/min. (56.0 A_{rms} and β = 73.0 deg)

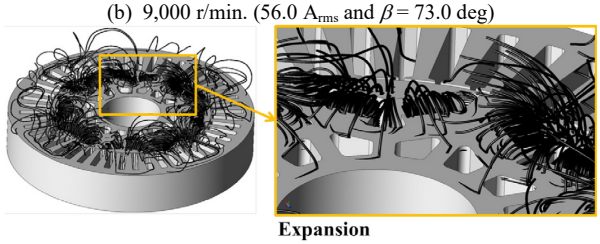

(c) 15,000 r/min. (127.0 A_{rms} and β = 81.5 deg)

Fig. 4. Three-dimensional magnetic flux lines simulated by FE-analysis.

case of motor with a bar-wound conductor coil as shown in Fig. 1, not only iron loss but also conductor eddy current loss due to spatial leakage flux is also concerned. However, it is difficult to directly measure this conductor eddy current loss separately from the copper loss caused by the fundamental content. Therefore, it is important to analyze this loss in detail using electromagnetic field analysis for the fuel consumption of electric vehicle.

C. Electromagnetic Field Analysis Method

In this section, among the experimental test results described in the previous section, it is clarified by large-scale electromagnetic field analysis what proportion of the conductor eddy current loss occupies in the total loss. As already mentioned, it is difficult to perform direct loss isolation of conductor eddy current losses. As a measurement method, first, a motor designed to have the same space factor using a flat wire of litz wire specification have to newly prepared. It is conceivable to measure the eddy current loss in bar-wound coil indirectly from the difference in temperature rise of the armature winding when driven under the same drive condition, that is the measurement of difference in Joule loss. However, since verification of analysis accuracy is the most important matter, it is the future study as the most important examination matter.

As an electromagnetic field analysis method in this paper, the parallel computing using domain decomposition method which is proposed in Ref. [10] was applied. Furthermore, this large-scale electromagnetic field analysis was conducted using the super computer that is K-computer of RIKEN in Japan. This super computer is capable of massively parallel computation [11]. Using the performance of K-computer, the electromagnetic field analysis in this paper was calculated in 480 parallels. To evaluate conductor eddy current loss separately from other losses, the following method was used in this analysis. The electromagnetic field analysis is calculated in two modeling methods, in the case where the current density inside the wire is forcibly made uniform and in the case where it is made ununiform. The former does not take the conductor eddy current into consideration by fixing the current density vector in the conductor by predefining the resistance value. On the other hand, in the latter, electrical conductivity is defined, and the direction and value of the current density vector are simultaneously executed with the calculation of the electromagnetic field distribution. The eddy current loss generated in the bar-wound coil can be elucidated from the difference between the above two analysis results. On the other hand, iron loss calculation is performed based on the classical iron loss calculation method. The eddy current loss coefficient k_e and the hysteresis loss coefficient k_h used for iron loss calculation are based on values measured in the past, and are in a map reference format so as to change depending of frequency and magnetic flux density. The k_e is defined in the range of 0.15 ~ 0.75 depending on the magnetic flux density and the frequency, and the k_h is similarly defined in the range of 51.2 ~ 243.2, respectively.

III. ELECTROMAGNETIC FIELD ANALYSIS RESULTS

A. Torque Analysis Accuracy

In this paper, detailed electromagnetic field analysis is performed at typical driving points listed in Table II. In this table, the rotation speed of 3,183 r/min is the operating point being driven at the base rotation speed and under MTPA control. On the other hand, since the rotation speeds of 9,000 r/min and 15,000 r/min are driven within the voltage limiting ellipse because of the field weakening region, the current phase is greatly advanced. Then, Table III compares the measured torque and the analysis torque at each drive point. From this table, it can be seen that the analysis accuracy is as high as about 10 % at rotation speeds of 3,183 r/min and 9,000 r/min. On the other hand, at a rotation speed of 15,000 r/min, the analysis value is over-calculated at a torque about 21.6 % higher than the measured value. It is considered that this factor

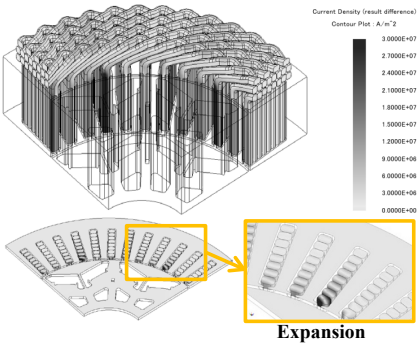

(a) 3,183 r/min. (137.3 A_{rms} and $\beta = 44.0$ deg)

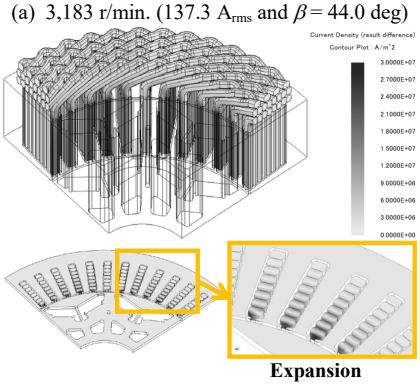

(b) 9,000 r/min. (56.0 A_{rms} and $\beta = 73.0$ deg)

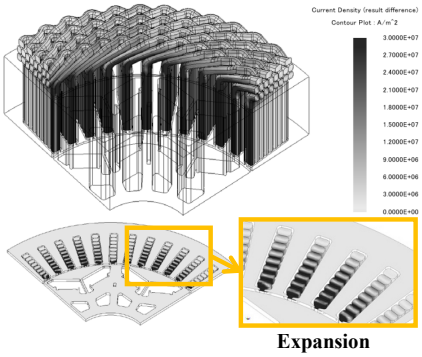

(c) 15,000 r/min. (127.0 A_{rms} and $\beta = 81.5$ deg)

Fig. 5. Conductor eddy current density distribution.

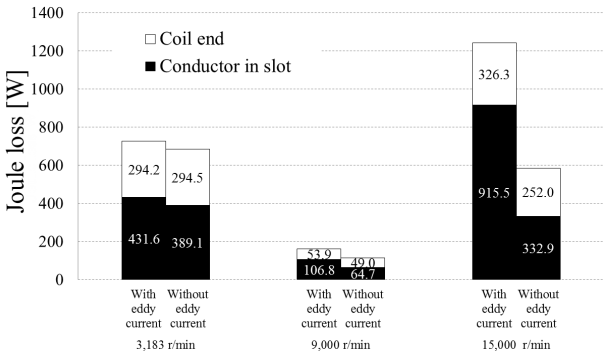

Fig. 6. Breakdown of conductor Joule loss with respect to rotation speed.

is due to iron loss analysis accuracy caused by time harmonics generated by the motor control factor. The analysis is simulated with a pure sinusoidal current source, but actually, this motor is controlled with rectangular voltage control at 15,000 r/min, it seems that the iron loss due to time harmonics is not counted. When simulating FE-analysis while considering the eddy current loss and satisfying sufficient convergence conditions, the electromagnetic field analysis model shown in Fig. 1 requires enormous analysis time even if the analysis method of Ref. [10] is used. In addition to this, increasing the number of analysis steps in order to consider time harmonics will result in unrealistic analysis time even with the supercomputer performance. This improvement method is for further study.

B. Spatial Leakage Magnetic Flux and Uniform Current in Armature Coil

Next, by visualizing the spatial leakage magnetic flux with electromagnetic field analysis, it is evaluated quantitatively the loss while understanding how the eddy current is generated in the bar-wound coil. Fig. 4 shows the results of visualizing the spatial leakage flux at each drive point in Table II. As can be confirmed from this figure, it can be seen that the spatial leakage magnetic flux increases as the current phase angle advances, as it is in the flux weakening region. As the current phase angle advances, the magnet flux and the armature flux face each other. Here, for the motor with a high torque density design, a magnet having a high coercive force is selected due to the thermal factor and the convenience of the reverse salient pole design. Therefore, the magnet flux leaks spatially in axial direction by opposing the two magnetic flux vectors. These result can also be confirmed by the visualization of the leakage flux in Fig. 4. Interlinking of the spatial leakage flux with the bar-wound conductor causes conductor eddy current loss. Then, it was confirmed by visualizing the eddy current density vector as shown in Fig. 5 as to how this leaked magnetic flux affects the current density distribution in the conductor by linking to the bar-wound coil. Here, the darker the color, the higher the conductor eddy current loss density. Since the eddy current density contour levels shown in Fig. 5 are made to coincide with each other, it can be seen that the contours become darker in proportion to rotation speed increases. Further, since the contour of the conductor portion in the stator slot is thickened from the same figure, the eddy current density in the conductor in the slot is also compared in the radial cross-sectional enlarged view. As a result, the difference in density of the conductor in the slot is significantly larger than the difference in density of the eddy current density in the conductor at the coil-end. In addition, from this figure, it can be confirmed that the conductor eddy current distribution is concentrated on the coil part enclosed into the slot, particularly in the vicinity of the air gap at the constant torque drive of 3,183 r/min. It is considered that the concentration of this current density is caused by the leakage magnetic flux which shorts between the stator teeth interlinking with the conductor. On the other hand, at 9,000 r/min and 15,000 r/min under the flux weakening region, it can be confirmed that the conductor eddy current distribution is also generated in the coil-end section. With respect to MTPA, in the flux weakening region, it can be confirmed that the distribution of the conductor eddy current is generated not only at the tip of the stator teeth but also in the stator. It is considered that the cause is that the amount of

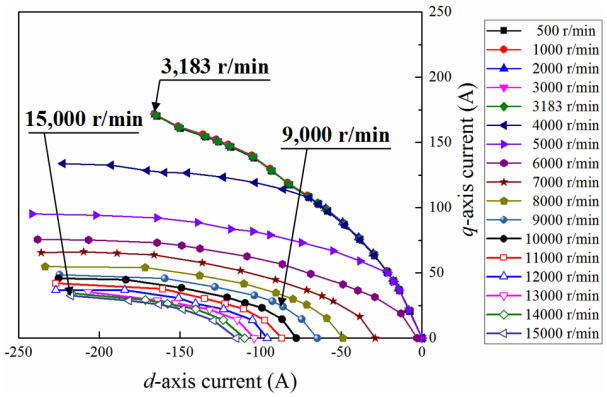

Fig. 7. Measured dq-axis current vector trajectory in motoring.

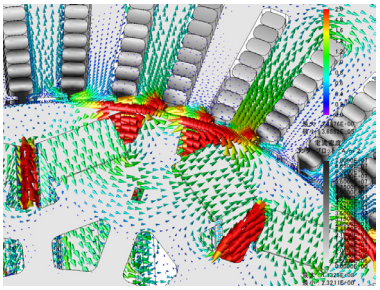

(a) Magnetic flux density vectors with β = 81.5 deg at 15,000 r/min.

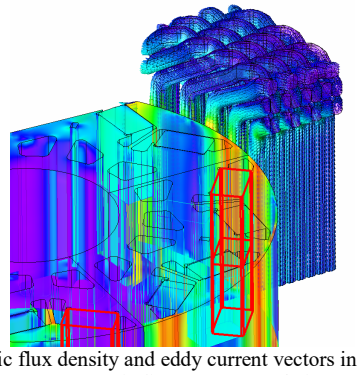

(b) Magnetic flux density and eddy current vectors in bar-wound armature windings at 15,000 r/min.

Fig. 8. FE-analysis results at 15,000 r/min.

magnetic flux shorting in the stator teeth is increased due to flux weakening control.

Next, when the bar-wound conductor is divided into two parts, the coil-end part and the inside of the slot, it is quantitatively evaluated what proportion of the conductor eddy current loss occupies at each part. The results are graphed in Fig. 6. For the purpose of grasping the conductor eddy current numerically, the analysis method described in Section II-C is used to make bar graphs for each case where the conductor eddy current is considered and not considered. From this figure, it can be confirmed that the Joule loss is increased by the generation of the conductor eddy current loss in addition to the copper loss at each drive point. Numerically, due to the conductor eddy current loss, the copper loss is 106.1 % at 3,183 r/min, the copper loss is 141.3 % at 9,000 r/min, and the copper loss is 212.3 % at 15,000 r/min, respectively. The conductor eddy current loss dramatically increases with respect to rotation speed increases. From this figure, it can be seen that the

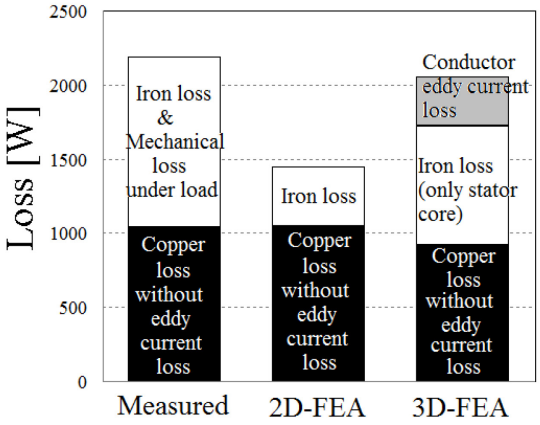

Fig. 9. Detailed loss analysis result at 15,000 r/min.

increase of the eddy current loss generated by the three-dimensional leakage flux in the conductor enclosed in the slots is more significant than that of the coil-end portion. Next, under the condition in which the conductor eddy current loss is taken into consideration, the copper loss is compared numerically between the conductor inside the slot and the conductor at the coil-end. Assuming that the copper loss in the slot is W_{cs} and the copper loss in the coil-end is W_{ce}, and evaluated as W_{cs} / W_{ce} for conductor eddy current loss effect analysis, W_{cs} /W_{ce} = 146.7 % at 3,183 r/min, W_{cs} / W_{ce} = 198.1 % at 9,000 r/min, and W_{cs} /W_{ce} = 280.6 % at 15,000 r/min, respectively. Fig. 7 shows the armature current vector trajectory with respect to rotation speed and load condition. Fig. 8 shows the magnetic flux density distribution and the current density distribution in the bar-wound coil at the rotation speed of 15,000 r/min. As can be seen from Fig. 7, at this rotation speed, it can be seen that the magnetic flux of the magnet and the armature magnetic flux are opposed to each other, and the magnetic flux crossing the stator teeth is generated. In particular, it can be confirmed that the large amount of leakage flux traverses between stator teeth in the vicinity of the air-gap. It can be seen that the leakage magnetic flux crossing between the stator teeth generates the conductor eddy current vector as shown in Fig. 8 (b).

C. Motor Loss Analysis

In this section, the ratio of the eddy current loss in bar-coils generated by the eddy current distribution visualized in the previous section to the total loss is grasped numerically. The iron loss was calculated with the analysis method in Section II-B. Fig. 9 shows the results of the iron loss compared with simulated values and measured values at 15,000 r/min. For the reference, the iron loss values calculated by two-dimensional magnetic field analysis are also included. The iron loss of actual measurement is calculated by the following method. The output power W_o is the result of converting the torque measured by a torque meter (T10FS manufactured by HBM) into an output. The copper loss W_c is a value calculated from the current measured by the power meter (WT1800) and the temperature-corrected winding resistance. The iron loss W_i is obtained by subtracting the sum of the mechanical loss at no-load and W_c from W_o. Therefore, it should be noted that the

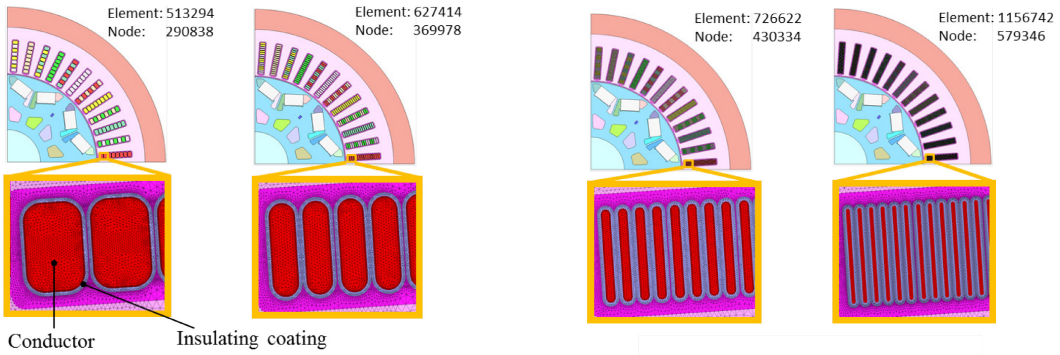

(a) Original. (b) Divided into 2. (c) Divided into 4. (d) Divided into 6.

Fig. 10. Bar-wound coil-split model in radial-direction.

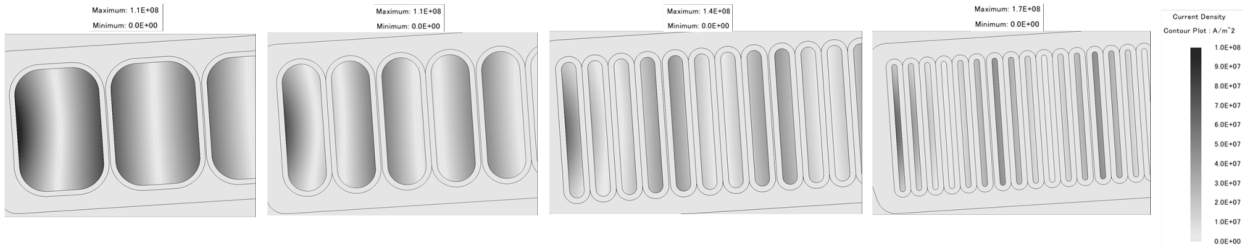

(a) Original. (b) Divided into 2. (c) Divided into 4. (d) Divide into 6.

Fig. 11. Current density distribution with respect to coil-divided number at 15,000 r/min. (radial direction)

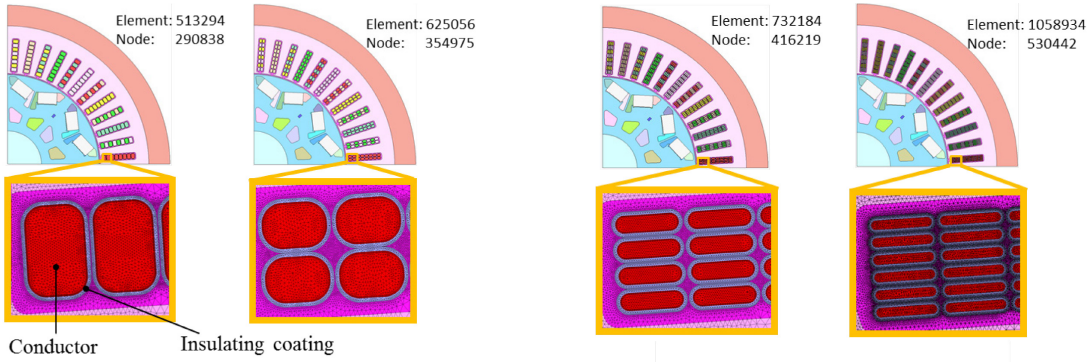

(a) Original. (b) Divided into 2. (c) Divided into 4. (d) Divide into 6.

Fig. 12. Bar-wound coil-split model in circumferential-direction.

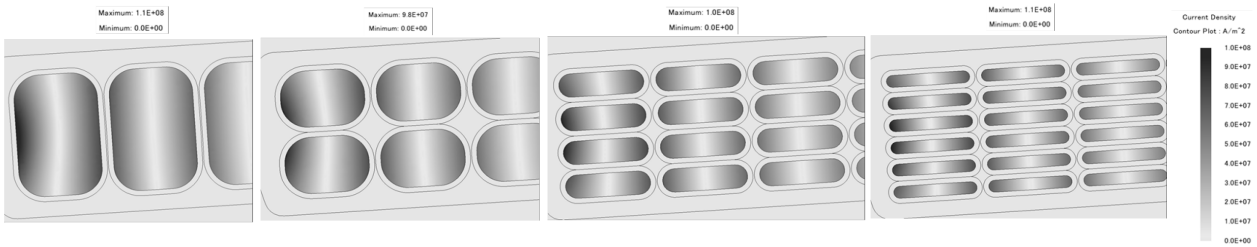

(a) Original. (b) Divided into 2. (c) Divided into 4. (d) Divide into 6.

Fig. 13. Current density distribution with respect to coil-divided number at 15,000 r/min. (circumferential direction)

measured core loss includes conductor eddy current loss and an increase in mechanical loss under load. Here, the separation of the conductor eddy current loss in the actual measurement is difficult to directly measure. For example, since it is necessary to measure indirectly from temperature rise etc., the measurement method will be a future work. According to Fig. 9, the total loss is closer to the actual measurement in the three-dimensional analysis than in the two-dimensional analysis. The difference between the three-dimensional analysis result and the actual measurement is considered to be because the iron loss due to the time harmonics caused by the PWM voltage is not taken into consideration. On the other hand, as a fact that becomes clear from Fig. 9, the conductor eddy current loss at 15,000 r/min is about 16 % of the total loss in 3D-FE analysis and can not be ignored.

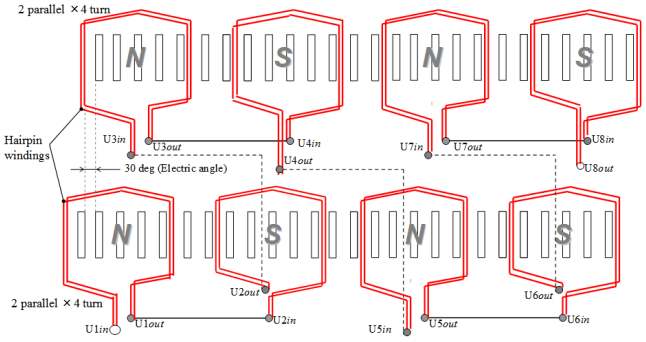

Fig. 14. U-phase coil connection diagram for 4-poles with dividing into 2 parallel.

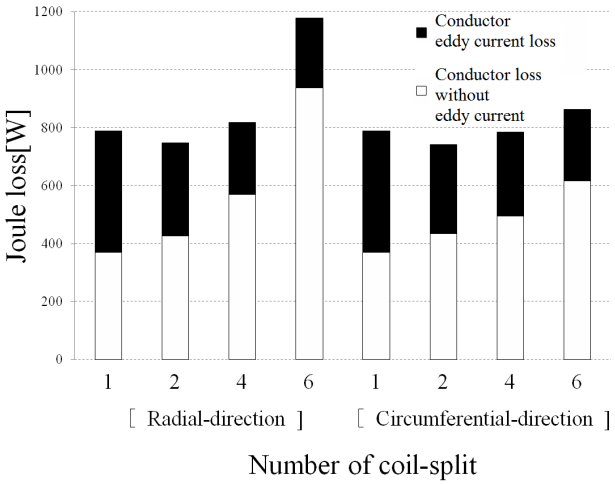

Fig. 15. Joule loss in bar-wound coil with respect to coil-split number.

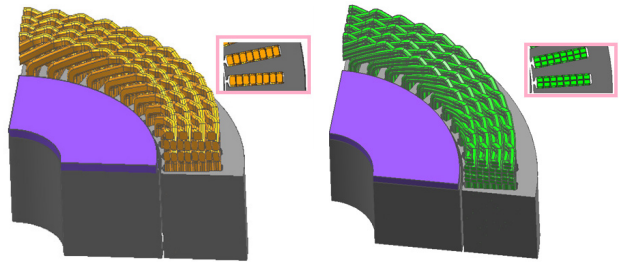

(b) Original model. (c) Model divided into 2 in the circumferential direction.

Fig. 16. Armature winding connection per pole.

(a) Pre-forming process. (b) Inserting process. (c) Welding process.

Fig. 17. Assembly procedure of bar-wound coil stator .

D. Preliminary Study of Conductor Eddy Current Loss Mitigation

The results in the previous section revealed that the conductor eddy current loss ratio in the conductor where is enclosed in the slot is large. As well-known knowledge, when the eddy current loss is generated in the conductor, the distribution of the main current flowing thorough the coil conductor becomes non-uniform due to the eddy current. In general, the skin thickness δ due to the skin effect can be expressed by Eq. (1). From this result, current concentrates on the edge of the portion close to the opening of the slot due to the harmonic magnetic flux.

$$\delta=\frac{1}{\sqrt{\pi f \mu \sigma}} \tag{1}$$

Here, f is a frequency, μ is a permeability, σ is an electrical conductivity, respectively.

In this section, basic research on conductor eddy current loss reduction is conducted by increasing the number of conductor divisions in the slot. In other words, it aims at shorting the eddy current path by dividing the cross-sectional area of the conductor into a lot of number. So, shortening the eddy current loss path can reduce the conductor eddy current loss, while the number of conductor divisions leads to an increase in the percentage of insulating coating on the conductor. As a result, when the number of divisions is excessively increased, the conductor cross-sectional area is reduced, and it is predicted that the copper loss is increased due to the increase in conductor resistance. In this preliminary study, the insulation coating thickness (0.1 mm) is not changed so that the withstand voltage performance does not change. There are two ways in which the number of coil divisions is increased in the circumferential direction and in the radial direction. Here, the relationship between the number of coil division and conductor copper loss is clarified by two-dimensional analysis for rapid simulation. Specifically, as shown in from Fig. 10 to Fig. 13, the number of divisions was changed to 2, 4 and 6 with respect to the original model of Fig. 1. Here, only the number of divisions of the armature coil is changed, and other design items such as the core shape are not changed. As shown in Fig. 14, the armature connection were made to increase in parallel with respect to the number of divisions increase. Thus, with respect to the original model of Fig. 1 (e), as shown in Fig. 14 (a), one hairpin winding is changed to two parallel connections with a cross-sectional area of approximately half.

Fig. 11 and Fig. 13 visualizes contour plots of the current density distribution at 15,000 r/min. Here, the darker the color, the higher the current density. From this figure, the partial concentration of the current density distribution can be reduced in proportion to the divided-number increases. The result of quantitatively evaluating the above is shown in Fig. 15. It can be numerically confirmed that the conductor eddy current loss can be reduced by increasing the number of coil divisions. On the other hand, the conductor resistance increases as the insulating coating ratio increases, and as a result, when the number of divisions is increased too much, the copper loss tends to increase. From these results, it is understood that the bisection of the coil results in a minimum of Joule loss of the bar-wound conductor. Furthermore, an interesting result is obtained from Fig. 15 that there is a difference in the increasing tendency of Joule loss between circumferential division and radial division. From this figure, it is understood that it is better to increase the number of divisions in the circumferential direction. The following two reasons can be considered. First,

it is a factor in the production of the bar conductor. Fig. 16 shows the original model and the 3D-CAD model divided in the circumferential direction. As shown in this figure, when the number of divisions increases more than two, the difficulty of forming and assembling the hairpin shape coil becomes remarkably high. In particular, if the number of divisions is increased in the radial direction, edgewise winding with the high aspect ratio, and there is a concern about damage to the insulating coating during pre-forming. Therefore, it is necessary to increases the thickness of the insulating coating as compared with the case of circumferential division. At this time, when increasing the number of divisions, the fillet at the corner of the coil is set to a constant value. When forming a rectangular copper wire, form a shape through a die and then apply an insulating coating. Thereafter, as shown in Fig. 17, the conductor bar coil is pre-formed into the hairpin shape by a forming jig, and then inserted into the stator slot, and the open side is welded to form a coil. In this process, it is necessary to make the fillet at the corner a certain value or more due to the restriction of mechanical strength when forming through tensioning and passing through a die and the restriction of insulation coating breakage protection at the time of pre-forming. As a result, in the case of increasing the number of divisions in the radial direction and in the case of increasing the number of divisions in the circumferential direction, differences occur in the wire cross section. This factor causes a difference in conductor resistance. The second factor is the difference in magnetic resistance to leakage flux passing through the slots. In particular, as visually confirmed in Fig. 5, the conductor eddy current loss in the slot is largely affected by the leakage flux passing through between the slots. Therefore, by increasing the number of divisions in the circumferential direction, the magnetic resistance becomes high due to the effect of the insulating coating against the leakage flux passing through the slots. From these facts, as for the effect on the number of divisions of the coil, it is understood that the Joule loss reduction effect is larger in the circumferential direction than in the radial direction. As described above, the effect of reducing the conductor eddy current loss by dividing the armature winding could be obtained. On the other hand, there is the concern that the circulating current may be generated when the gap between the rotor and the stator due to eccentricity occurs or when the three-phase current becomes unbalanced. In the future, it will be necessary to consider the above effects.

IV. Conclusion

In this paper, in the permanent magnet type synchronous motor using the bar-wound conductor coil for low voltage hybrid vehicles, visualization and quantitative evaluation of the eddy current generated in the bar-wound coil were performed. Using the CAE model that faithfully reproduces the coil formation of the actual machine, it was clarified how the spatial leakage flux changes with respect to *dq*-axis current vector. Furthermore, when the coil was divided into two parts, the coil-end part and the part contained in the slot, the latter revealed that the eddy current loss was larger. Then, the try to reduce conductor eddy current loss, it is confirmed that the effect of changing the number of divisions in the circumferential direction or radial direction is confirmed by CAE, and it was revealed that the method of dividing into two in the circumferential direction is the most effective.

Future plans are to pursue in depth the specific method of reducing the conductor eddy current loss of the bar-wound coil while incorporating various factors, e.g., circulating current suppression and manufacturability that were not considered in this preliminary study.

References

[1] F. Momen, K. Rahman, Y. Son and P. Savagian, "Electrical Propulsion System Design of Chevrolet Bolt Battery Electric Vehicle," *IEEE Energy Conversion Congress and Expo* (*ECCE*) 2016.

[2] K. Rahman, S. Jurkovic, P. J. Savagian, N. Patel and R. Dawsey, "Retrospective of Electric Machines for EV and HEV Traction Applications at General Motors," in *Proc. IEEE 2016 Energy Conversion Congress and Exposition* (*ECCE*), 2016.

[3] T. Ishigami, Y. Tanaka and H. Homma, "Motor Stator with Thick Rectangular Wire Lap Winding for HEVs," *IEEE Trans. on IA*., 2015, vol. 51, no. 4, pp. 2917-2923.

[4] F. Momen, K. Rahman and Y. Son, "Electric Propulsion System Design of Chevrolet Bolt Battery Electric Vehicle," *IEEE Trans. on IA*. vol. 55, no. 1, 2018.

[5] J.H. Seo, T. K. Chung, C. G. Lee, S. Y. Jung and H. K. Jung, "Harmonic Iron Loss Analysis of Electrical Machines for High-Speed Operation Considering Driving Condition," *IEEE Trans. on Magnetics,* vol. 45, no. 10, pp. 4656-4659, 2009.

[6] I. Suehiro, T. Mifune, T. Matsuo, J. Kitao, T. Komatsu and M. Nakano, "Ladder Circuit Modeling of Dynamic Hysteretic Property Representing Excess Eddy-Current Loss," *IEEE Trans. on Magnetics,* vol. 54, no. 3, 2017.

[7] M. Paradkar and J. Bocker, "Analysis of Eddy Current Losses in the Stator Windings of IPM Machines in Electric and Hybrid Electric Vehicle Applications," in *Proc. 8th IET Internatiional Conference on Power Electronics, Machines and Drives* (PEMD2016)*,* 2016.

[8] J. Kitao, Y. Takeda, Y. Takahashi, K. Fujiwara, A. Ahagon, T. Matsuo, "Loss Calculation Method Considering Hysteretic Property with Play Model in Finite Element Magnetic Field Analysis," *IEEE Trans. on Magnetics,* vol. 50, no. 2, 2014.

[9] T. Matsuo, M. Miyamoto, "Dynamic and Anisotropic Vector Hysteresis Model Based on Isotropic Vector Play Model for Nonoriented Silicon Steel Sheet," *IEEE Trans. on Magnetics,* vol. 48, no. 2, pp. 215-218, 2012.

[10] K. Semba, K. Tani, T. Yamada, T. Iwashita, Y. Takahashi and H. Nakashima, "Parallel Performance of Multithreaded ICCG Solver Based on Algebraic Block Multicolor Ordering in Finite Element Electromagnetic Field Analysis," *IEEE Trans. on Magnetics,* vol. 49, no. 5, pp. 1581-1584, 2013.

[11] H. Miyazaki, Y. Kusano, N. Shinjou, F. Shoji, M. Yokokawa, and T. Watanabe, "Overview of the K-computer System," FUJITSU Scientific & Technical Journal, vol. 48, no. 3, pp. 255-265, July, 2012.

Masahiro Aoyama (M'13-) was born in Shizuoka Japan, 1984. He received the B.S. degree in electrical and electronic engineering from Nagaoka Univerisity of Technology in 2006, and the M.S. degree in electrical and electronics engineering from the Toyota Technical Institute, Japan, in 2008, respectively.

From 2008 to 2018, he was a Researcher with SUZUKI Motor Corporation. Since 2018, he has been an

Assistant Professor with Shizuoka University. His research interests include electric machines, especially permanent magnet-free motor and variable magnetic flux motor for automotive applications.

Jianing Deng was born in China, 1986. He received the B.S. and M.S. degrees in electrical and electronic engineering from Saga University, Japan, in 2010.

From 2010 to 2018, he was a Researcher with SUZUKI Motor Corporation. Since 2018, he has been a Researcher with Denso Corporation. His research interests include electric machines, especially permanent magnet synchronous motor for automotive applications.